Surface Science 641 (2015) 289–293

Contents lists available at ScienceDirect

Surface Science

journal homepage: www.elsevier.com/locate/susc

Acetaldehyde partial oxidation on the Au(111) model catalyst surface: C–C bond activation and formation of methyl acetate as an oxidative coupling product

Mustafa Karatok [a], Evgeny I. Vovk [a,b], Asad A. Shah [a], Abdurrahman Turksoy [a], Emrah Ozensoy [a,*]

[a] Chemistry Department, Bilkent University, 06800 Bilkent, Ankara, Turkey
[b] Boreskov Institute of Catalysis, 630090 Novosibirsk, Russian Federation

ARTICLE INFO

Available online 11 April 2015

Keywords:
Au(111)
Oxidative coupling
Partial oxidation
Acetaldehyde
Methyl acetate

ABSTRACT

Partial oxidation of acetaldehyde (CH_3CHO) on the oxygen pre-covered Au(111) single crystal model catalyst was investigated via Temperature Programmed Desorption (TPD) and Temperature Programmed Reaction Spectroscopy (TPRS) techniques, where ozone (O_3) was utilized as the oxygen delivery agent providing atomic oxygen to the reacting surface. We show that for low exposures of O_3 and small surface oxygen coverages, two partial oxidation products namely, methyl acetate (CH_3COOCH_3) and acetic acid (CH_3COOH) can be generated without the formation of significant quantities of carbon dioxide. The formation of methyl acetate as the oxidative coupling reaction product implies that oxygen pre-covered Au(111) single crystal model catalyst surface can activate C–C bonds. In addition to the generation of these products; indications of the polymerization of acetaldehyde on the gold surface were also observed as an additional reaction route competing with the partial and total oxidation pathways. The interplay between the partial oxidation, total oxidation and polymerization pathways reveals the complex catalytic chemistry associated with the interaction between the acetaldehyde and atomic oxygen on catalytic gold surfaces.

1. Introduction

Gold has been considered as an inactive metal in catalysis for a long time. However, several pioneering studies in the last few decades demonstrated the unusual catalytic properties of gold nanoparticles in oxidation reactions which paved the way to a vast number of subsequent catalytic studies establishing the reactivity of gold-based systems in a variety of oxidation, hydrogenation, dehydrogenation and coupling reactions [1–15]. Heterogeneous gold catalysts can be structurally-tuned to demonstrate a high selectivity in partial oxidation reactions eluding the generation of undesirable oxidation byproducts as well as the total oxidation product, CO_2 [15,16]. Therefore, the high selectivity of gold catalysts in heterogeneous catalytic reactions also renders these materials promising systems in green chemistry applications. In order to optimize the performance of these uniquely active and selective catalytic materials, mechanisms of the corresponding reactions occurring on gold surfaces should be understood at the molecular level. Fundamental surface science studies on single crystal gold model catalysts provide valuable insights regarding the reaction mechanisms operating during the catalytic reactions [17–23]. Selective oxidation and oxidative coupling reactions of alcohols and aldehydes can produce commercially valuable partial oxidation products such as esters which are of high demand by the chemical industry. Furthermore, carrying out such partial oxidation reactions at a gas/solid interface over Au heterogeneous catalysts eliminates the necessity to employ environmentally toxic solvents and expensive post-reaction separation processes associated with homogenous catalytic alternatives.

It has been pointed out in former studies that in order to obtain particular partial oxidation products on gold catalysts, specific reaction intermediates must be initially formed on the catalyst surface [24]. Due to their strongly basic and highly reactive nature, adsorbed atomic oxygen species are very efficient in initiating the formation of such surface intermediates [15,25]. However, oxygen delivery and activation on gold surfaces using conventional oxidants (e.g. O_2) may present challenges as the dissociative adsorption probabilities of many oxygen carriers on gold surfaces are extremely low [26–28]. In order to circumvent the oxygen activation problem on monometallic gold surfaces, several methods have been devised enabling the decoration of catalytic gold surfaces with adsorbed atomic oxygen species [20]. One of these effective methods to prepare atomic oxygen on gold surfaces under ultra-high vacuum (UHV) conditions is ozone (O_3) exposure [29].

Thus, in the current report, we focus on the oxidative coupling reactions of acetaldehyde on the Au(111) single crystal model catalyst surface. By exploiting O_3(g) as an efficient oxygen delivery agent, we elucidate the nature of the catalytic products generated as a result of

* Corresponding author.
E-mail address: ozensoy@fen.bilkent.edu.tr (E. Ozensoy).

http://dx.doi.org/10.1016/j.susc.2015.04.005
0039-6028/

the interaction between pre-adsorbed oxygen species on Au(111) and acetaldehyde via surface-sensitive mass spectrometric techniques.

2. Materials and methods

Experiments were performed in a custom-made UHV chamber with a base pressure of 4×10^{-10} Torr which is equipped with X-ray Photoemission Spectroscopy (XPS, Riber Mg/Al dual anode with a Riber EA150 electron energy analyzer), Low Energy Electron Diffraction (LEED, custom-made), Infrared Reflection Absorption Spectroscopy (IRAS, Bruker Tensor 37) and Temperature Programmed Desorption (TPD)/Temperature Programmed Reaction Spectroscopy (TPRS) capabilities. A quadrupole mass spectrometer (Ametek Dycor Dymaxion DM200) and a PID-controlled linear sample heater (Heatwave, Model 101303) were used for the TPD and TPRS experiments. All of the temperature-programmed mass spectroscopic experiments were performed using a heating rate of 1 K/s. Au(111) single crystal sample (10 mm-diameter × 1 mm-thickness disc, both sides polished, MaTeck GmbH) was affixed on Ta wires; through which the sample could be resistively heated up to 1073 K. The cooling of the sample was achieved via a liquid nitrogen reservoir located inside the sample manipulator probe holding the Au(111) single crystal. The temperature of the sample was measured using a K-type thermocouple attached on the lateral facet of the Au(111) disc. Au(111) sample surface was cleaned by cycles of Ar^+ sputtering (Ar(g), Linde AG, >99.999% purity) at room temperature using an accelerating voltage of 1.5 kV which is followed by annealing at 773 K in UHV. The cleanness of the surface prior to experiments was confirmed by XPS and LEED.

Atomic oxygen was accumulated on the Au(111) model catalyst surface by ozone exposure at 140 K. This dosing temperature was found to be the lowest temperature allowing the clean delivery of ozone from the silica-gel with a minimum accumulation of water and deposition of contaminants from the ozone source on the Au(111) model catalyst surface. Ozone was produced on-board by feeding O_2(g) (Linde AG, >99.999% purity) to a commercial ozone generator (Genozon, GN-G1001S); the generated ozone was initially trapped and concentrated in a silica gel (1–2 mm mesh) which was positioned in a glass cell that is placed in a dry ice/ethanol slurry kept at ca. 200 K. Then the trapped ozone in the silica gel was released in a controlled manner into the dosing line by gradual heating of the ozone trap. Released ozone from the trap was dosed to the UHV system via a home-made pinhole-doser. The pinhole doser was manufactured by punching a circular hole (diameter = ca. 5 μm) on a ¼″-diameter blank stainless steel Swagelok VCR gasket using a high-power pulsed-laser. It is worth emphasizing that this pinhole doser was instrumental for the efficient delivery of ozone to the UHV system and by extension to the Au(111) single crystal sample surface. Utilization of such a tool significantly hinders the decomposition of the ozone during the delivery allowing the transfer of intact O_3(g) on the sample surface. Before the experiments, acetaldehyde (Sigma-Aldrich, anhydrous, purity ≥99.5%) was additionally purified by multiple freeze–thaw–pump cycles in the gas manifold. Acetaldehyde was introduced onto the oxygen pre-covered Au(111) surface (O/Au(111)) at 90 K. In the rest of the text, exposures of adsorbate species (ε) are given in Langmuir (L, 1 L = 1×10^{-6} Torr·s) and the estimated surface coverages of the corresponding adsorbates are reported in monolayer equivalents (MLE).

3. Results and discussion

Before the investigation of the interaction between adsorbed oxygen species with acetaldehyde on the Au(111) model catalyst surface, it is instructive to examine the adsorption/desorption phenomena corresponding to each of the reactants in an individual manner. Thus, Fig. 1 presents the TPD data corresponding to the dissociative O_3(g) adsorption on the clean Au(111) surface at 140 K for various exposures of O_3(g), which is used to create atomic oxygen species on

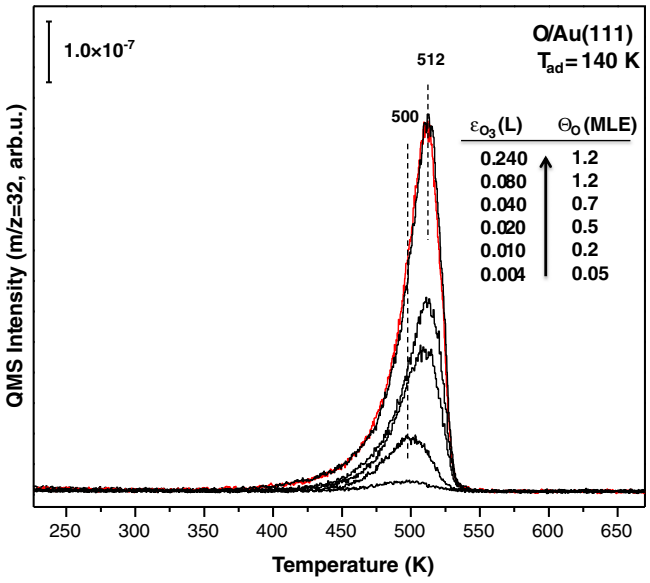

Fig. 1. Coverage-dependent TPD profiles for the m/z = 32 (O_2) desorption channel obtained via ozone (O_3(g)) decomposition on the clean Au(111) model catalyst surface at 140 K.

Au(111) with different surface coverages. In these set of TPD experiments, recombinative desorption of atomic oxygen in the form of O_2 was followed by monitoring the m/z = 32 desorption channel. It is worth mentioning that other relevant desorption channels such as m/z = 16 (due to the fragmentation of O_2/O_3), 18 (H_2O), 28 (CO), 44 (CO_2), and 48 (O_3) were also simultaneously monitored (data not shown). However, no other significant desorption signals were obtained other than m/z = 16 and 32. Comparative analysis of the m/z = 16 and 32 channels indicated that both of these desorption channels were associated with the O_2 evolution.

TPD data given in Fig. 1 corresponding to the O_2 deposition from the oxygen pre-covered Au(111) surface suggest that there are two distinct desorption regimes evident by the temperature maxima located at 500 and 512 K. While the former desorption maximum is associated with low surface coverages of oxygen, the latter is associated with high surface coverages. These distinct types of oxygen desorption signals might be related to chemisorbed oxygen, surface oxide and/or bulk oxide species [20]. The adsorption of oxygen on Au model catalyst surfaces is a complex phenomenon, where the interplay between the nature of the oxygen species, surface dispersion of oxygen, oxygen diffusion to the subsurface, reconstruction and oxidation of the metallic surface layer closely depends on the experimental parameters such as the adsorbate coverage and the surface temperature [30]. The nature of the various surface oxygen species generated on the Au(111) model catalyst surface, their role in partial oxidation reactions as a function of surface temperature and adsorbate coverage will be discussed in detail in a forthcoming report [31]. TPD studies by Saliba et al. [29] revealed that O_3 exposure on the Au(111) surface at 300 K leads to O_2 desorption maxima located at 520 and 550 K for low and high coverages; respectively. In this former TPD study, a heating rate of $8.5\ K \cdot s^{-1}$ was employed in the TPD experiments. Thus, the discrepancy in the O_2 desorption maxima between the current results given in Fig. 1 and that of Saliba et al. [29] can be readily attributed to the differences in the surface temperature of Au(111) during adsorption and the heating ramp rate.

As can be seen from the Fig. 1, the Au(111) surface can be saturated with ozone at a surface temperature of 140 K. This is evident by the observation that two of the highest O_3 exposures used in the current TPD experiments (i.e. ε = 0.080 and 0.240 L) lead to an identical integrated O_2 desorption signal. These two particular surfaces correspond to an Au(111) model catalyst surface which is decorated with the highest

atomic oxygen coverage obtained via ozone exposure at 140 K. This is consistent with a former report by Saliba et al. [29] where the maximum atomic oxygen coverage on Au(111) via ozone exposure was estimated to be $\theta_O = 1.2$ MLE using TPD and Auger Electron Spectroscopy (AES). Along these lines, in our atomic oxygen surface coverage estimations, we estimated θ_O values using this reference atomic oxygen saturation coverage of 1.2 MLE.

As another benchmark experiment, we investigated the adsorption and desorption properties of acetaldehyde on the clean Au(111) model catalyst surface. Detailed analysis of the coverage-dependent adsorption behavior of acetaldehyde on the clean Au(111) model catalyst surface at 90 K is given in Fig. 2. The TPD results presented in Fig. 2 are in very good agreement with the former work of Pan et al. [32]. Based on this former report, 117 K and 124 K desorption features in Fig. 2 can be attributed to the molecular desorption of acetaldehyde from multilayer states, where the former feature can be associated with an amorphous acetaldehyde multilayer while the latter corresponds to a crystalline multilayer phase. The characteristic desorption signal at 139 K can be assigned to the desorption of acetaldehyde from the first monolayer on the Au(111) surface. On the other hand, the high temperature desorption signal located at c.a. 194 K is associated with the depolymerization of the polymerized forms of acetaldehyde on the Au(111) model catalyst surface [32]. It is worth mentioning that polymerization of acetaldehyde has been reported on a variety of single crystal surfaces where the polymerization was confirmed by TPD and/or High Resolution Electron Energy Loss Spectroscopy (HREELS) on Ru(001) [33], Pt(111) and Sn/Pt(111) [34], and Ag(111) [35], while acetaldehyde polymerization was not observed on Pd(111) [36].

As can be seen in Fig. 2, relative acetaldehyde coverages present on the Au(111) surface can be calibrated using the 139 K desorption signal corresponding to the molecular acetaldehyde in the first monolayer. By considering the maximum integrated desorption signal that can be attained by the 139 K (i.e. monolayer) peak in the absence of any multi-layer features located at 124 or 117 K, one can estimate the approximate saturation coverage of adsorbed species in the first monolayer. This can be achieved by integrating the m/z = 29 TPD curve between 128 and 223 K at the particular exposure corresponding to a maximum intensity of the 139 K feature (i.e. $\varepsilon_{CH3CHO} = 0.010$ L). This approach is based on the presumption that during the completion of the first monolayer, albeit a limited extent, polymeric states start to appear before the saturation of the monolayer feature at 139 K.

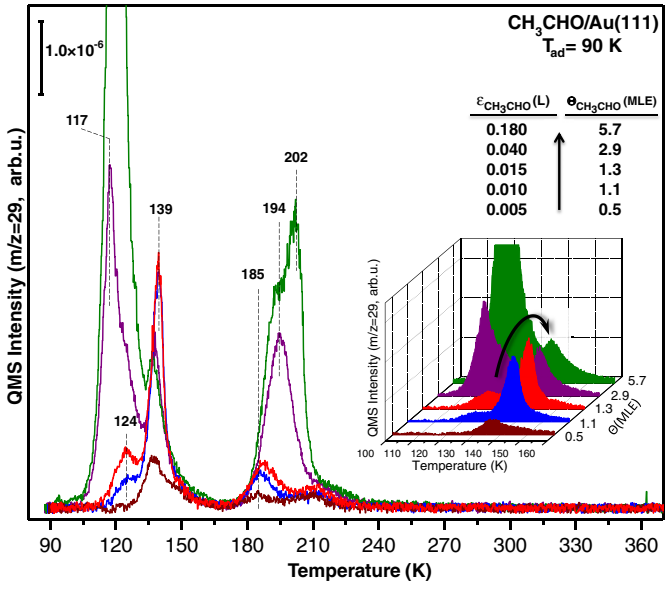

Fig. 2. Coverage-dependent TPD profiles for the m/z = 29 desorption channel obtained via acetaldehyde ($CH_3CHO(g)$) adsorption on the clean Au(111) model catalyst surface at 90 K. Inset emphasizes the non-monotonic intensity of the chemisorbed acetaldehyde desorption feature at 139 K as a function of acetaldehyde coverage (see text for details).

Along these lines, the interplay between the monolayer desorption feature at 139 K and the polymerization-related desorption states located at 185, 194 and 202 K in Fig. 2; is worth discussing in further detail. It is plausible that during the completion of the first monolayer, two-dimensional (i.e. 2D) polymeric acetaldehyde species [33] may be formed in addition to the adsorbed acetaldehyde species. This particular 2D-polymeric state has a characteristic decomposition temperature of 185 K. As can be seen in the inset of Fig. 2, at high acetaldehyde surface coverages exceeding a monolayer, intensity of the 139 K feature starts to attenuate at the expense of the growth of the multilayer features (i.e. 124, 117 K) along with new and strong desorption signals at 194 and 202 K. Therefore, it can be argued that at high surface coverages of acetaldehyde on Au(111), polymerization starts to dominate which lead to the formation of strongly bound three-dimensional (3D) [33] polymeric species, decomposing and desorbing at elevated temperatures (i.e. at 194 and 202 K).

Having investigated the separate adsorption behavior of the individual reactants, we also studied the adsorption of one of the important oxidative coupling products that can be generated during the reaction of acetaldehyde with oxygen pre-covered Au(111), namely methyl acetate (CH_3COOCH_3, MA). As can be seen in Table 1, the main QMS fragmentation signal for MA is observed for m/z = 43. Thus, we performed coverage-dependent TPD experiments on the clean Au(111) surface at 90 K by varying the MA exposure (Fig. 3) and monitoring the m/z = 43 desorption signal. Fig. 3 indicates that low exposures of MA on Au(111) lead to a characteristic desorption feature at ca. 167 K. This particular desorption feature can be assigned to the molecular adsorption of MA on Au(111) in the first monolayer. It is apparent that 167 K desorption signal saturates for higher MA exposures. At higher exposures (e.g. 0.01 L), a weak desorption feature can be detected at 141 K, which can be assigned to MA species originating from the second layer. Further increase in the MA exposure results in the observation of two multiyear desorption features at 135 and 137 K which can be attributed to crystalline and amorphous multilayer phases, respectively.

Next, the reaction between the oxygen pre-covered Au(111) single crystal model catalyst surface with acetaldehyde was investigated via TPRS. Fig. 4 presents the corresponding TPRS results where a clean Au(111) surface was initially dosed with O_3 at a surface temperature of 140 K with an exposure of $\varepsilon_{O3} = 0.004$ L. This was followed by a 0.04 L acetaldehyde exposure at 90 K. Relevant desorption channels (i.e. m/z = 18, 28, 29, 32, 43, 44, 45 and 59) were simultaneously monitored during the temperature-programmed reaction. Analysis of the normalized relative QMS fragmentation patterns given in Table 1 suggests that m/z = 18, 28, 29, 45, 59 desorption channels can almost exclusively be explained by considering a single species for each desorption channel (i.e. H_2O, CO, CH_3CHO, CH_3COOH and CH_3COOCH_3; respectively). On the other hand, m/z = 44 desorption channel can be associated with both CH_3CHO and CO_2 species. At least three separate species can simultaneously contribute to the m/z = 43 desorption channel; namely CH_3CHO, CH_3COOH and CH_3COOCH.

In Fig. 4, the desorption peaks located at 141 appearing in multiple desorption channels such as m/z = 28, 29, 43 and 44 can be predominantly due to the chemisorbed acetaldehyde in agreement with similar TPD features located at 139 K in Fig. 2. Fig. 4 reveals a water desorption signal located at 154 K. Since this feature is not accompanied by concomitant carbon-containing desorption features of similar magnitude appearing at 154 K; it is likely that this particular water desorption signal is associated with background water accumulated on the surface at low temperatures during the experiment. Similar water desorption signals at 154 K have been observed after individual adsorption of acetaldehyde and methyl acetate (not shown). Desorption features located at 171 K in Fig. 4 particularly for the m/z = 29, 43 and 59 desorption channels can be assigned to predominantly MA, the oxidative coupling product. It is worth mentioning that since the m/z = 44 trace in Fig. 4

Table 1
Fragmentation patterns in the mass spectroscopic Residual Gas Analysis (RGA).

	Normalized QMS Fragmentation Intensities					
Chemical name	m/z = 28	m/z = 29	m/z = 43	m/z = 44	m/z = 45	m/z = 59
Acetaldehyde* (CH_3CHO)	–	100	17	29	–	–
Methyl acetate* (CH_3COOCH_3)	–	9	100	3	–	5
Ethyl acetate** ($CH_3COOC_2H_5$)	2	12	100	3	15	–
Acetic acid** (CH_3COOH)	4	8	100	2	90	–
Diethyl ether**,*** ($(C_2H_5)_2O$)	5	43	8	2	45	67
Carbon dioxide** (CO_2)	10	–	–	100	1	–
Carbon monoxide** (CO)	100	1	–	–	–	–

For each particular chemical, relative fragmentation intensity of the most intense desorption channel was normalized to 100.
* Current results.
** Obtained from [37].
*** The most intense fragmentation channel of diethyl ether (i.e. m/z = 31) is not shown in the table as this channel was not utilized in the current TPD/TPRS experiments.

does not reveal an intense feature at 171 K, a significantly high contribution of acetaldehyde to this feature can be ruled out. Furthermore, desorption of MA at 171 K during the reaction of oxygen pre-covered Au(111) with acetaldehyde (Fig. 4) is in perfect agreement with the desorption temperature of chemisorbed MA on the clean Au(111) model catalyst surface as shown in Fig. 3. On the other hand, the significant CO desorption signal located at 171 K can be attributed to the decomposition of chemisorbed acetaldehyde species into CO and H_2 (the latter species was not followed in the current TPRS experiments) [33]. This is due to the fact that neither MA nor acetaldehyde species has an intense QMS fragmentation signals at m/z = 28. One can note that ethyl acetate (like methyl acetate) also has an intense m/z = 43 fragmentation signal (see Table 1) and can be considered as an alternative product. However, lack of the m/z = 45 signal at 171 K which is an expected fragmentation signal for ethyl acetate (Table 1), suggests that a significant amount of ethyl acetate formation in addition to MA can be ruled out. Furthermore, our control experiments involving individual ethyl acetate adsorption on the clean Au(111) single crystal surface showed that for adsorbate coverages less than 1 ML, ethyl acetate desorbs at a temperature of 189 K with a first-order desorption kinetics (data nor shown).

This particularly higher desorption temperature of ethyl acetate is also in accordance with the interpretation that the 171 K feature in the m/z = 43 trace of Fig. 4 is predominantly associated with MA rather than ethyl acetate. It is worth mentioning that oxidation of acetaldehyde on oxygen-precovered Au(111) surface was also studied by X. Liu et al. [38], however MA was not detected as a reaction product, since in this former work, acetaldehyde was adsorbed on Au(111) at 180 K, a temperature which is higher than the MA desorption temperature from Au(111).

Fig. 4 shows that at higher temperatures, TPRS data reveal a distinct desorption feature at 226 K for the m/z = 45 channel which is exclusively associated with acetic acid. It is worth mentioning that this particular feature cannot be attributed to diethyl ether; since there is no detectable feature in the m/z = 59 TPRS channel of Fig. 4 at 226 K (Table 1). The influence of the acetic acid desorption is also visible in other relevant desorption traces such as m/z = 29, 43, 44. However behavior of m/z = 29, 43, 44 at T ≥ 200 K is more complex due to the contribution to these desorption channels from the desorption products of polymerized acetaldehyde species as well as decomposed acetic acid [39]. On the other hand, the desorption signals appearing at 237 K in

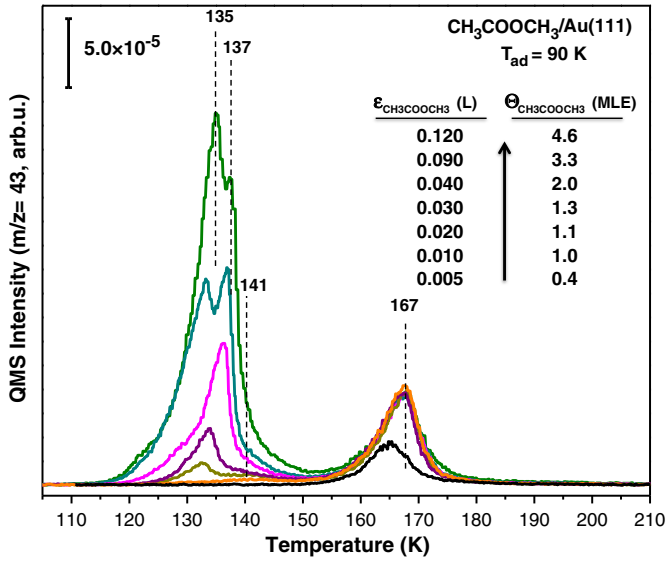

Fig. 3. Coverage-dependent TPD profiles for the m/z = 43 desorption channel obtained via methyl acetate (CH_3COOCH_3(g)) adsorption on the clean Au(111) model catalyst surface at 90 K.

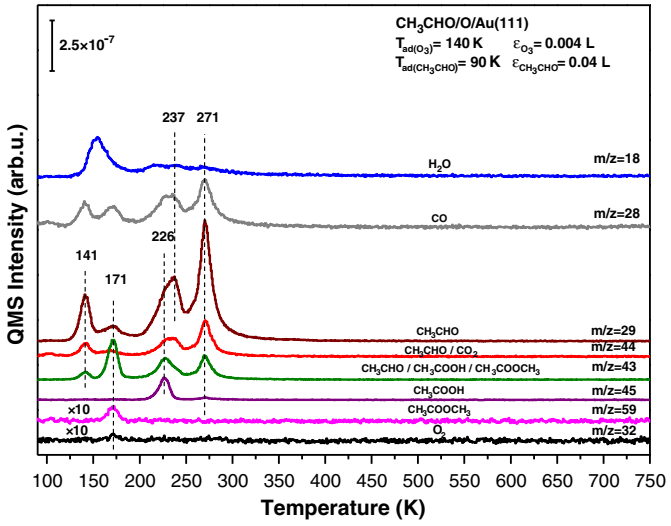

Fig. 4. TPRS profiles for various desorption channels obtained after the exposure of 0.004 L of ozone on a clean Au(111) model catalyst surface at 140 K, followed by 0.04 L acetaldehyde exposure at 90 K.

m/z = 28, 29, 43, 44 traces of Fig. 4 have a smaller contribution from acetic acid due to the lack of the m/z = 45 desorption signal and reflect a convoluted identity that can be associated with acetaldehyde and CO_2. However, the lack of a significant H_2O desorption signal (i.e. m/z = 18 in Fig. 4) within the temperature window of 200–300 K suggests that total oxidation is not significant under such reaction conditions. Finally, increasing the reaction temperature to 271 K leads to the evolution of strong desorption signals which can be originating from the decomposition of polymerization products of acetaldehyde as well as the decomposition of acetic acid. It is worth mentioning that no significant O_2 (i.e. m/z = 32) desorption was detected throughout the TPRS experiments given in Fig. 4.

4. Conclusions

In the current work, partial oxidation of acetaldehyde (CH_3CHO) on the oxygen pre-covered Au(111) single crystal model catalyst was investigated via Temperature Programmed Desorption (TPD) and Temperature Programmed Reaction Spectroscopy (TPRS), where ozone (O_3) was utilized as the oxygen delivery agent to the surface. We show that for low exposures of O_3 and small surface oxygen coverages, two different partial oxidation products namely, methyl acetate (CH_3COOCH_3) and acetic acid (CH_3COOH) can be generated without the formation of significant quantities of carbon dioxide. Since the formation of methyl acetate as the oxidative coupling reaction product implies C–C bond activation; it was demonstrated that oxygen pre-covered Au(111) single crystal model catalyst surface can activate C–C bonds. In addition to the generation of these products; indications of the polymerization of acetaldehyde on the gold surface were also observed as an additional catalytic route competing with the partial and total oxidation pathways. The interplay between the partial oxidation, total oxidation and polymerization pathways reveals the complex catalytic chemistry associated with the interaction between the acetaldehyde and atomic oxygen on catalytic gold surfaces.

Acknowledgment

Authors acknowledge the financial support from the Scientific and Technological Research Council of Turkey (TUBITAK) (Project code: 112T589). Authors also gratefully acknowledge Prof. Mehmet Erbudak (ETH Zurich, Physics Department) for his contributions regarding the construction of the UHV experimental setup and Prof. Ömer İlday (Bilkent University, Physics Department) for his help with the production of the pin-hole doser. E.I. Vovk acknowledges the financial support from the Scientific and Technological Research Council of Turkey (TUBITAK) (Program code: 2221).

References

[1] G.C. Bond, P.A. Sermon, G. Webb, D.A. Buchanan, P.B. Wells, J. Chem. Soc. Chem. Commun. 444 (1973).
[2] G.J. Hutchings, J. Catal. 96 (1985) 292.
[3] M. Haruta, T. Kobayashi, H. Sano, N. Yamada, Chem. Lett. 16 (1987) 405.
[4] M. Valden, X. Lai, D.W. Goodman, Science 281 (1998) 1647.
[5] M.S. Chen, D.W. Goodman, Science 306 (2004) 252.
[6] M. Boronat, A. Leyva-Pereza, A. Corma, Acc. Chem. Res. 47 (3) (2014) 834.
[7] X. Liu, L. He, Y. Liu, Y. Cao, Acc. Chem. Res. 47 (3) (2014) 793.
[8] I.X. Green, W. Tang, M. Neurock, J.T. Yates Jr., Acc. Chem. Res. 47 (3) (2014) 805.
[9] A. Wittstock, M. Baumer, Acc. Chem. Res. 47 (3) (2014) 731.
[10] D. Widmann, R.J. Behm, Acc. Chem. Res. 47 (3) (2014) 740.
[11] M.S. Ide, R.J. Davis, Acc. Chem. Res. 47 (3) (2014) 825.
[12] S. Yamazoe, K. Koyasu, T. Tsukuda, Acc. Chem. Res. 47 (3) (2014) 816.
[13] M. Pan, A.J. Brush, Z.D. Pozun, H.C. Ham, W.-Y. Yu, G. Henkelman, G.S. Hwanga, C.B. Mullins, Chem. Soc. Rev. 42 (2013) 5002.
[14] C. Marsden, E. Taarning, D. Hansen, L. Johansen, S.K. Klitgaard, K. Egeblad, C.H. Christensen, Green Chem. 10 (2008) 168.
[15] B. Xu, R.J. Madix, C.M. Friend, Acc. Chem. Res. 47 (3) (2014) 761.
[16] A. Wittstock, V. Zielasek, J. Biener, C.M. Friend, M. Baumer, Science 327 (2010) 319.
[17] X. Deng, C.M. Friend, J. Am. Chem. Soc. 127 (2005) 17178.
[18] B.K. Min, C.M. Friend, Chem. Rev. 107 (2007) 2709.
[19] R.A. Ojifinni, N.S. Froemming, J. Gong, M. Pan, T.S. Kim, J.M. White, G. Henkelman, C.B. Mullins, J. Am. Chem. Soc. 130 (2008) 6801.
[20] J. Gong, Chem. Rev. 112 (2012) 2987.
[21] K.J. Stowers, R.J. Madix, C.M. Friends, J. Catal. 308 (2013) 131.
[22] C.G.F. Siler, T. Cremer, J.C.F. Rodriguez-Reyes, C.M. Friend, R.J. Madix, ACS Catal. 4 (2014) 3281.
[23] M. Pan, J. Gong, G. Dong, C.B. Mullins, Acc. Chem. Res. 47 (2014) 750.
[24] T. Cremer, C.G.F. Siler, J.C.F. Rodriguez-Reyes, C.M. Friend, J. Phys. Chem. Lett. 5 (2014) 1126.
[25] D. Outka, R. Madix, J. Am. Chem. Soc. 109 (1987) 1708.
[26] J.J. Pireaux, M. Chtaib, J.P. Delrue, P.A. Thiry, M. Liehr, R. Caudano, Surf. Sci. 141 (1984) 211.
[27] A.G. Sault, R.J. Madix, Surf. Sci. 169 (1986) 347.
[28] B. Xu, X. Liu, J. Haubrich, C.M. Friend, Nat. Chem. 2 (2010) 61.
[29] N. Saliba, D.H. Parker, B.E. Koel, Surf. Sci. 410 (1998) 270.
[30] B. Xu, C.M. Friend, Faraday Discuss. 152 (2011) 307.
[31] E.I. Vovk, M. Karatok, A.A. Shah, A. Turksoy, V.I. Bukhtiyarov, E. Ozensoy, Active and Inactive Oxygen in Methanol Oxidation on Au(111), 2015. (in preparation).
[32] M. Pan, D.W. Flaherty, C.B. Mullins, J. Phys. Chem. Lett. 2 (2011) 1363.
[33] M.A. Henderson, Y. Zhou, J.M. White, J. Am. Chem. Soc. 111 (1989) 1185.
[34] H. Zhao, J. Kim, B.E. Koel, Surf. Sci. 538 (2013) 147.
[35] W.S. Sim, P. Gardner, D.A. King, J. Am. Chem. Soc. 118 (1996) 9953.
[36] J.L. Davis, M.A. Barteau, J. Am. Chem. Soc. 111 (1989) 1782.
[37] http://webbook.nist.gov/chemistry/.
[38] X. Liu, B. Xu, J. Haubrich, R.J. Madix, C.M. Friend, J. Am. Chem. Soc. 131 (2009) 5757.
[39] Y.X. Li, M. Bowker, J. Catal. 142 (2) (1993) 630.